Supplementary Information for

Ultrathin 3R-MoS_2 metasurfaces with atomically precise edges for efficient nonlinear nanophotonics

George Zograf[1,†], Betül Küçüköz[1], Alexander Yu. Polyakov[1], Abhay V. Agrawal[1], Maria Bancerek[2], Witlef Wieczorek[3], Tomasz J. Antosiewicz[1,2], Timur O. Shegai[1,‡]

[1]Department of Physics, Chalmers University of Technology, 412 96, Göteborg, Sweden
[2]Faculty of Physics, University of Warsaw, Pasteura 5, 02-093, Warsaw, Poland
[3]Department of Microtechnology and Nanoscience, Chalmers University of Technology, Göteborg, 412 96, Sweden
[†]email: georgii.zograf@chalmers.se
[‡]email: timurs@chalmers.se

Contents

Optical experiments.

Second-harmonic generation spectra and power dependence.

To measure SHG intensity using avalanche photodiode (APD) we perform SHG spectroscopy to confirm the signal shape, spectral position ($\lambda_{pump}/2$), and a lack of background signal. Figure S1a demonstrates SHG spectra of the 3R-MoS_2 flake excited with the pump wavelength $\lambda_{pump} = 1000$ nm at different pump powers ranging from 0.1 mW to 2.25 mW.

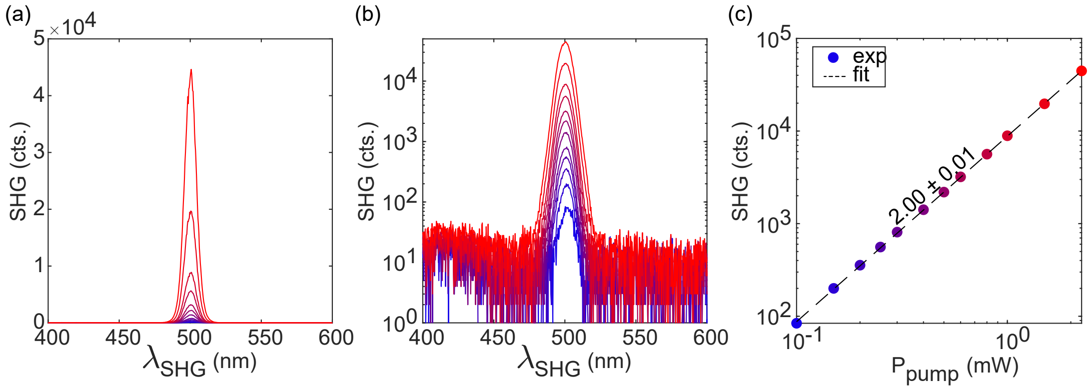

Figure S1: SHG spectroscopy of the 3R-MoS_2 flake. (a) SHG spectra of the flake at different pump powers from 0.1 mW to 2.25 mW in linear scale, obtained using 1000 nm excitation wavelength. (b) The same as in (a) but in the logarithmic scale. (c) Signal power – to pump power log-log dependence showing the slope of 2 and indicating the output signal is indeed due to SHG.

Spectrally the SHG signal is stable and has no visible signs of artificial signals or excessive background noise. The logarithmic scale of the SHG intensity in Figure S1b confirms the negligible intensity of the background compared to the main SHG peak even at the lowest pump power 0.1 mW (blue line).

Additional confirmation of the SHG nature of the signal is a quadratic dependence of the intensity as a function of the pump power. Figure S1c depicts the log-log dependence of the SHG intensity as a function of increased pump powers from 0.1 mW to 2.25 mW. The linear fit in such a logarithmic scale reveals a nearly perfect second-order nonlinearity slope - 2.00 ± 0.01, proving the presence of a clean SHG signal.

Back-focal plane spectroscopy and microscopy.

The optical reflection experiments of 3R-MoS_2 metasurfaces were carried out with the help of back-focal plane microscopy and spectroscopy setup which is schematically shown in Fig. S2a. The broadband white light illumination generated by the laser-driven light source excites the metasurfaces through high NA = 1.49 oil immersion objective to gain access to k-vector values exceeding the free space k_0 value. The reflected light passes the Bertrand lens placed in the back focal plane of the high NA objective. Such configuration allows to resolve the Fourier image of the reflected light from the metasurface. The example of the Fourier image is shown in Fig. S2b,c. To analyze the spectra at every point in the BFP plane we adjusted a fiber bundle consisting of 19 optical fibers coupled to the spectrometer. Such a bundle allows one to collect simultaneously spectral information at separated points. To cover the whole Fourier plane with fiber bundle we have adjusted a mechanical microscrew that allows to precisely move the fiber bundle in k_x/k_y plane allowing to collect both TE and TM polarizations.

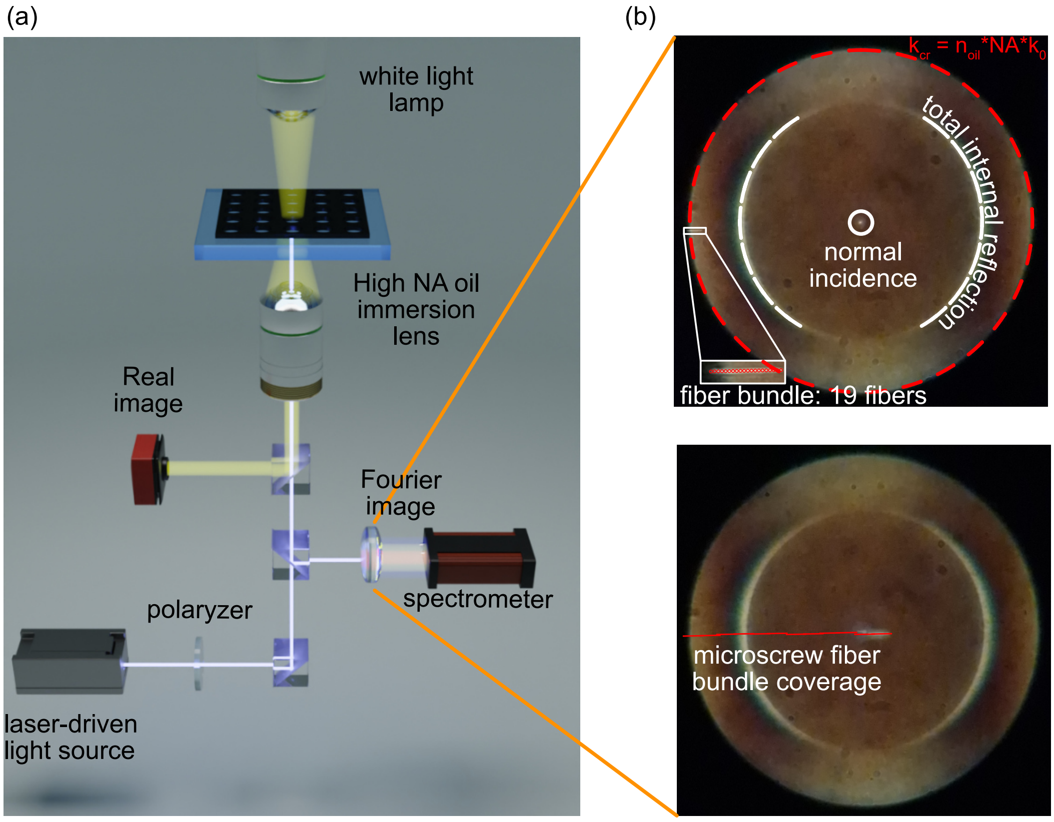

Figure S2: Back-focal plane spectroscopy and microscopy. (a) Schematic of the BFP experimental setup. (b) Fourier images in the back focal plane of the metasurface on a glass substrate. Red dashed line indicates the critical k-vector that is reachable via oil immersion. White dashed line indicates the total internal reflection angle. White box magnifies the positioning of the fiber bundle consisting of 19 fibers in the back focal plane. Each individual fiber is shown with red circle.

Sample morphology.

Scanning electron microscopy analysis of nanopatterned MoS_2 samples.

The exact parameters of the metasurfaces play a crucial role in achieving high-Q states [1]. The holes size analysis is shown in the main text, while the pitch size estimation is demonstrated in Fig. S3, where the pitches in x and y axis $\Lambda_{x,y}$ distributions are shown.

The pitch size along the x-axis (blue areas) and pitch along the y-axis (red boxes) are slightly mismatched. One of the reasons is the line-by-line scanning in SEM. The error bars in the legends of the figures are statistical error bars calculated from the mean value and the standard deviation of the pitch distributions.

3R- *vs.* 2H-MoS_2 etching, stacking faults in 3R-MoS_2, and influence of Espacer on SEM of circular 3R-MoS_2 metasurface.

During the wet-etching procedure, the pre-exposed MoS_2 flakes with circular holes tend to modify the hole shape into atomically sharp holes that follow the crystalline structure of the flake exclusively along the zigzag direction. The 3R stacking that has broken inverse symmetry generates atomically sharp triangles that are shown in Fig. S4a,b, where SEM image of the 3R-MoS_2 flake is shown. The crystalline broken inverse symmetry results in the broken inverse symmetry hole shape – an equilateral triangle, which can also indicate the nature of the crystalline structure and stacking order.

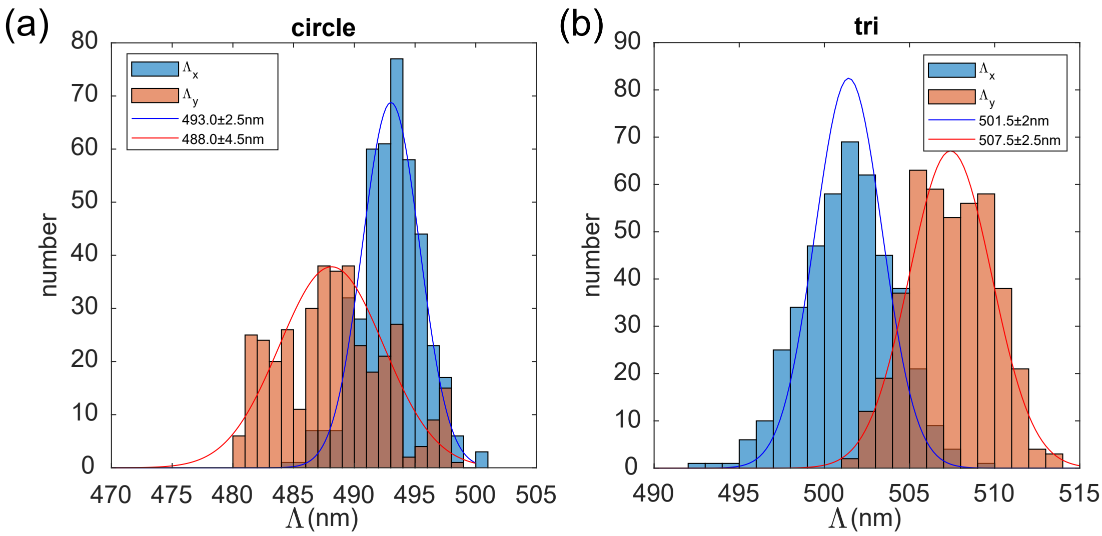

Figure S3: Pitch analysis of the sample. (a) Pitch size histograms in x and y directions of the circle hole metasurface

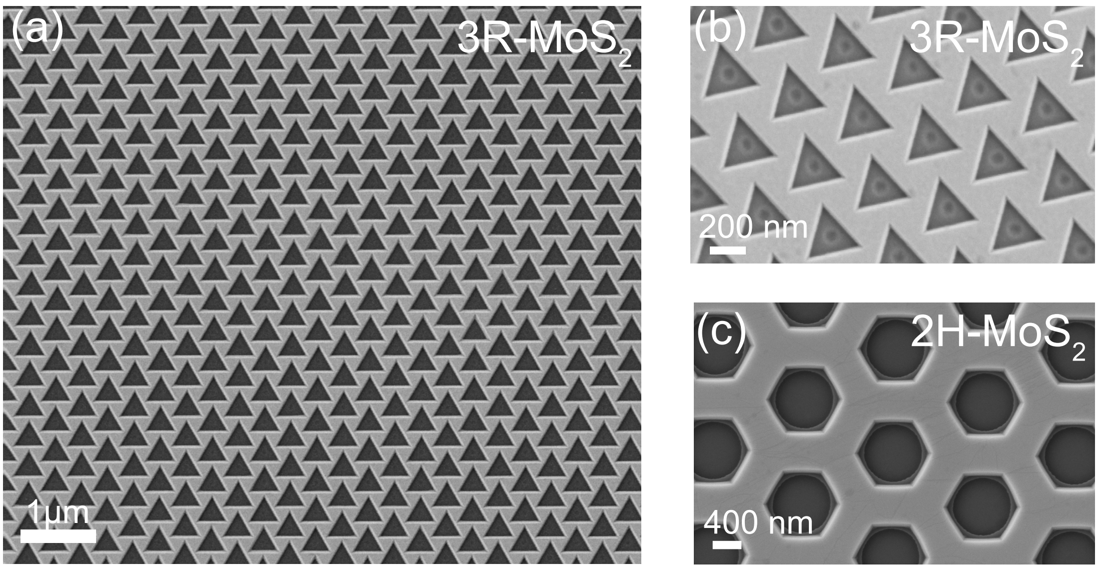

Figure S4: Wet etching of 3R- *vs.* 2H-MoS_2 multilayers. (a) SEM image of a wet-etched 3R-MoS_2 flake. The scale bar is 1 μm. (b) Tilted SEM image of an atomically sharp triangular hole in a wet-etched 3R-MoS_2 flake. Circular holes are lithographically made as seed holes for wet-etching into triangular holes. The scale bar is 200 nm. (c) SEM image of the wet-etched 2H-MoS_2 flake with initial circular seed holes. The scale bar is 400 nm.

Contrary to the 3R phase, the 2H lacks the broken inversion symmetry, thereby lacks bulk quadratic nonlinearity, during the very same wet-etching protocol creates atomically sharp hexagons (Fig. S4c) manifesting the preserved in plane mirror symmetry as described in previous works [2, 3].

Such wet etching can be used not only to create atomically sharp meta-atoms for optical metasurfaces, but also to study the stacking order of the flake without optical nonlinear experiments, TEM, or other atomic structure analysis, simply by wet etching the circular holes in the host flake.

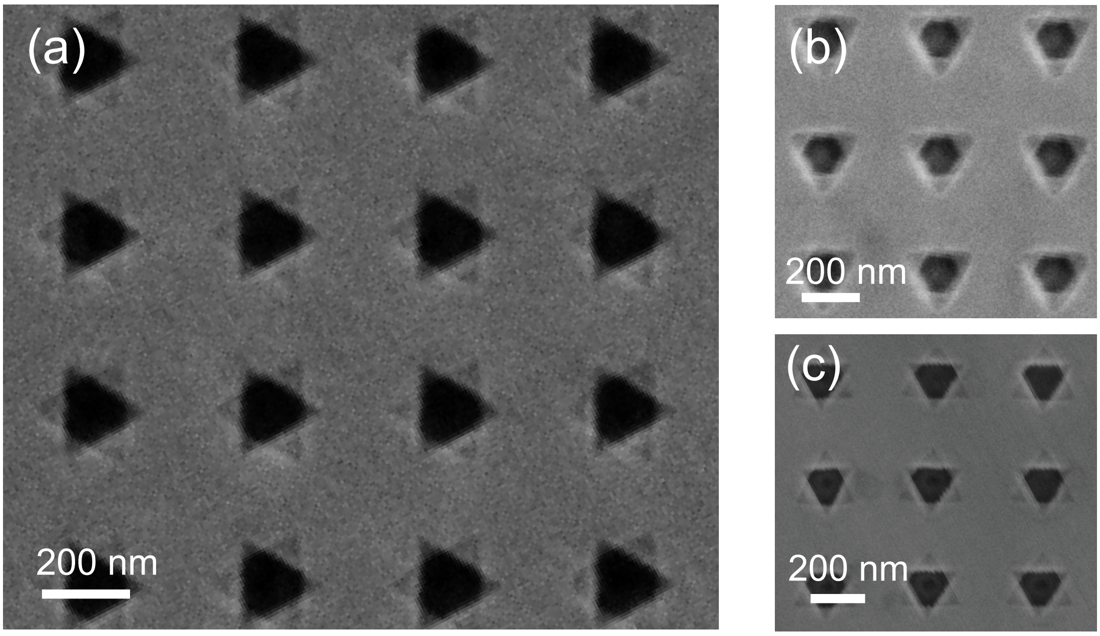

Figure S5: Stacking faults in multilayer 3R-MoS_2 flakes. (a-c) Stacking faults appearance in various 3R-MoS_2 flakes. These faults appear either as truncated triangles or as hexagonal nanoholes, suggesting the presence of two oppositely oriented triangles, which, in turn, is indicative of AB (typical for pure 2H-TMD multilayers) instead of AA' stacking (typical for pure 3R-TMD multilayers). These stacking faults are challenging to identify in pristine 3R-MoS_2 flakes. However, our wet etching method facilitates their observation by forming characteristic geometrical shapes. Pure stacking-fault-free 3R-MoS_2 multilayers result in ideal triangular nanoholes, as shown in the main text.

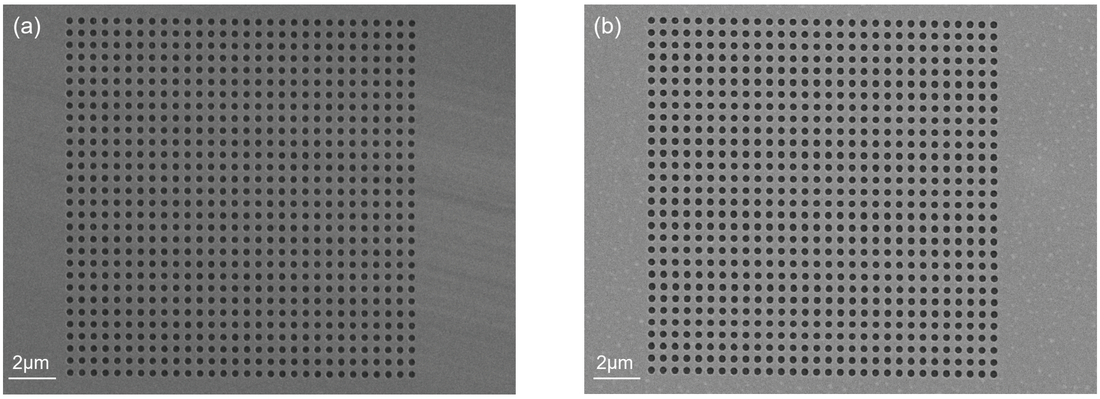

Figure S6: SEM images before and after Espacer coating. (a) Low-magnification SEM image of the metasurface array on a glass substrate before optical measurements, showing a clean surface and well-defined circular metasurface array. (b) After completing all optical measurements, an Espacer was spin-coated onto the sample conductive layer to take higher-resolution SEM images, which are used in the main text for circular hole analysis. The Espacer introduced carbon particles around the array, which notably were *not* present during the optical measurements, and therefore did not degrade their quality.

References

[1] Kühne, J. *et al.* Fabrication robustness in BIC metasurfaces. *Nanophotonics* **10**, 4305–4312 (2021).

[2] Munkhbat, B. *et al.* Transition metal dichalcogenide metamaterials with atomic

precision. *Nat. Commun.* **11**, 4604 (2020).

[3] Dewambrechies, A., Polyakov, A. Y., Küçüköz, B. & Shegai, T. O. Enhanced second-order nonlinearities at strained ultrasharp zigzag edges in multilayer MoS_2. *J. Phys. Chem. C* **127**, 15395–15405 (2023).